Journal of
Synchrotron
Radiation

ISSN 0909-0495

Received 10 September 2009
Accepted 18 October 2009

Artificial neural networks applied to the analysis of synchrotron nuclear resonant scattering data

N. Planckaert,* J. Demeulemeester, B. Laenens, D. Smeets, J. Meersschaut, C. L'abbé, K. Temst and A. Vantomme

Instituut voor Kern- en Stralingsfysica and INPAC, KU Leuven, Celestijnenlaan 200 D, BE-3001 Leuven, Belgium. E-mail: nikie.planckaert@gmail.com

The capabilities of artificial neural networks (ANNs) have been investigated for the analysis of nuclear resonant scattering (NRS) data obtained at a synchrotron source. The major advantage of ANNs over conventional analysis methods is that, after an initial training phase, the analysis is fully automatic and practically instantaneous, which allows for a direct intervention of the experimentalist on-site. This is particularly interesting for NRS experiments, where large amounts of data are obtained in very short time intervals and where the conventional analysis method may become quite time-consuming and complicated. To test the capability of ANNs for the automation of the NRS data analysis, a neural network was trained and applied to the specific case of an Fe/Cr multilayer. It was shown how the hyperfine field parameters of the system could be extracted from the experimental NRS spectra. The reliability and accuracy of the ANN was verified by comparing the output of the network with the results obtained by conventional data analysis.

Keywords: nuclear resonant scattering; artificial neural networks; data analysis.

1. Introduction

The use of X-rays for the investigation of the structural and electronic properties of condensed matter has expanded tremendously since the advent of third-generation synchrotron sources. Together with the increasing brilliance of X-ray sources, the quantity of experimental data generated at synchrotron facilities has developed at a pace even higher than that of the X-ray flux. Since large amounts of spectra can be measured in shorter and shorter time periods, there is an increasing need to develop computer codes that allow for a fast data analysis, without manual intervention by the user. Moreover, in order to make fast online decisions during the experiment on what course to follow, novel data analysis systems should be created that can treat experimental data in real time. One technique that can particularly benefit from such a fast and online analysis environment is nuclear resonant scattering (NRS) of synchrotron radiation. Since its development in 1985 (Gerdau *et al.*, 1985), NRS has evolved from an exotic technique in the field of spectroscopy to a widely used tool for the investigation of magnetic, structural and dynamical properties of matter *via* hyperfine interactions (Röhlsberger, 2004). A direct interpretation of the NRS spectra, however, is obstructed by the complexity of the data, from which the relevant physical parameters can often only be extracted after a detailed quantitative analysis of the measurements. So far, this analysis has been carried out by comparing theoretically calculated spectra with the measured data, and adjusting the parameters of the calculations to obtain the best agreement between theory and data. Although several interactive fitting routines have been developed for this purpose (Sturhahn, 2000; Shvyd'ko, 1999), intensive and laborious human initiative, creativity and intervention is required to evaluate the spectra.

Since the development of NRS with synchrotron radiation, alternative experimental set-ups have been proposed to enhance the interpretability of the data by transforming the conventional NRS spectra, usually recorded in a time differential mode, to energy domain (Sturhahn, 2001; Callens *et al.*, 2005). In this work we present a different approach to achieve an instantaneous data analysis in NRS experiments, namely by making use of artificial neural networks (ANNs). These are program codes that are developed to solve specific problems by relating numerous possible inputs to the corresponding output parameters, without the implementation of the physics determining the problem (Bishop, 1995). Fig. 1 shows the typical architecture of an ANN, which basically consists of an input and output node array that are connected through several hidden node layers in between. The nodes of each layer are mutually connected with the nodes of the neighbouring layer(s) and transfer data with a weight which is specific for each connection. The output of a single node is a function of the summed and weighted inputs from the previous node layer. The transfer weights need to be determined in order to adapt the network to the particular issue. The adjustment of these weights is called the training. Once

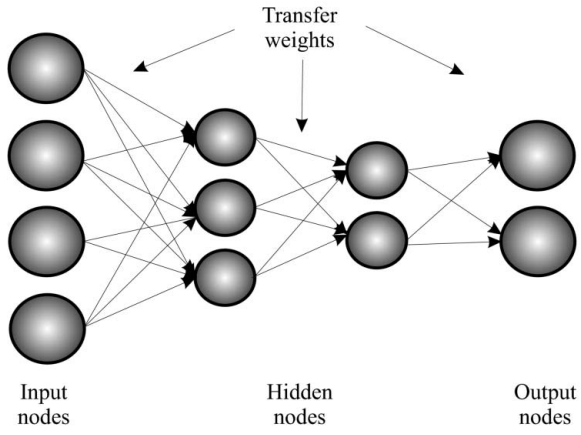

Figure 1
Schematic drawing of an artificial neural network.

the weights of the network are set, the developed ANN can be used to directly relate a given input (in our case the NRS spectra) to the corresponding output (the relevant physical parameters) and the network is considered trained to solve the particular problem.

In order to teach the ANN how to relate specific features of the data to specific properties of the sample, the 'supervised learning' method is applied (Bishop, 1995). In supervised learning a so-called 'training set' is created, which consists of several thousands of spectra, either real data or theoretically calculated spectra, with well known output parameters. When the data of the training set are presented to the input of the network, having its weights initially set to random, the output parameters of the ANN can be calculated. These parameters are connected to the desired output parameters by means of a network error E, which is given by

$$E = \frac{1}{2}\sum_{n=1}^{N}(y_n - o_n)^2. \quad (1)$$

In this summation, which runs over the number of specimens in the training set, y is the calculated output of the network (for reasons of simplicity only a single output is considered) and o is the desired or correct output. To train the network, the network error is minimized by consecutively adjusting the weights of all successive layers after each training iteration by means of a backpropagation algorithm (Bishop, 1995). Simultaneously, a network error is calculated on another similar but independent test set containing spectra not presented to the network in the training phase. This is necessary to avoid the well known problem of 'overtraining', in which the ANN is overfitted to the training data but loses its generalization capabilities. Once a minimal error is reached on both the training set and the test set, the training of the network is completed and the ANN can be applied to the experimental data set.

While the creation of the training set and the initial training itself are time-consuming, once a trained network is obtained thousands of experimental spectra can be analyzed almost instantaneously. Up to now, artificial neural networks have been successfully applied to several experimental techniques, including Rutherford backscattering spectrometry (Barradas & Vieira, 2000; Barradas *et al.*, 2002), infrared spectroscopy (Duponchel *et al.*, 1999) and Mössbauer spectroscopy (Paulsen *et al.*, 2000; De Souza *et al.*, 2002). The aim of this work is to validate the capability of ANNs for the NRS data analysis. As a specific test system, an Fe/Cr multilayer is presented, for which the measured data will be analyzed both by conventional analysis and by means of a specifically developed ANN.

2. NRS of synchrotron radiation

NRS of synchrotron radiation finds its origin in the Mössbauer effect (Mössbauer, 1958), which describes the resonant absorption and subsequent re-emission of photons by the nuclear levels of atoms bound in a solid. After scattering of the synchrotron photons from a nuclear resonant absorber, the system returns to its initial state, and the intensity of the resonantly emitted photons is detected as a function of time after the excitation by the synchrotron pulse. For an isolated nucleus, only a single transition between ground and excited nuclear level is possible, and the temporal evolution of the nuclear resonant scattered intensity can be described by an exponential decay, with a time constant determined by the lifetime of the excited nuclear level. When the atom is embedded in a crystal, however, the degeneracy of the nuclear levels will be lifted owing to hyperfine interactions, and different transitions between ground state and excited state become possible. Owing to the broad bandwidth of the synchrotron radiation, all transitions will be excited simultaneously and the coherent decay of the excited nuclear levels will give rise to a periodic interference pattern, caused by the energy differences between the various nuclear transitions. These oscillations, known as quantum beats, are superimposed on the exponential decay of the nuclear resonant scattered intensity (Fig. 2).

The shape of the NRS spectrum is a fingerprint of the local magnetic and electronic environment in which the nucleus is embedded. For a magnetic interaction, for instance, the beat period is inversely proportional to the total magnetic field at the position of the nucleus. This is illustrated in Fig. 2, where NRS spectra were calculated for a ^{57}Fe absorber, characterized by a hyperfine field of -17 T [Figs. 2(a) and 2(c)] and -33 T [Figs. 2(b) and 2(d)]. As can be observed in the simulations, the shape of the NRS spectrum is also sensitive to the direction of the magnetic hyperfine field, since the orientation of the magnetic field determines the number of frequencies that contribute to the quantum beat pattern. When the in-plane angle θ between the hyperfine field and the σ-vector of the incoming radiation is changed, the shape of the NRS spectrum evolves from a single frequency pattern for $\theta = 90^\circ$ [Figs. 2(a) and 2(b)] to a multiple frequency spectrum for $\theta = 0^\circ$ [Fig. 2(c) and 2(d)].

For the relatively simple example of a single hyperfine field, the hyperfine parameters can be extracted in a rather straightforward manner from the shape of the NRS spectra.

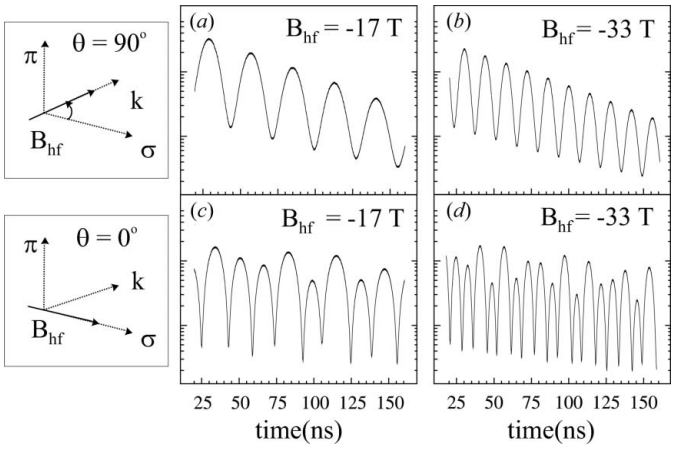

Figure 2
Time spectra of NRS from a ^{57}Fe absorber, for selected directions and magnitudes of the magnetic hyperfine field B_{hf}. The spectra were calculated using the *CONUSS* code (Sturhahn, 2000). k is the incident photon direction, whereas σ and π form the linear polarization basis of the synchrotron radiation. The in-plane angle between the hyperfine field B_{hf} and the σ-vector of the incoming radiation is given by the angle θ.

However, when the hyperfine fields are distributed in magnitude and/or direction, several parameters will influence the shape of the spectrum, resulting in complicated interference patterns (Röhlsberger *et al.*, 2001, 2002). A minor change of one of the hyperfine parameters, driven by external conditions such as pressure, strain or magnetic fields, will drastically modify the entire spectrum, so that the measurements can only be interpreted after a quantitative analysis of the data.

3. Fe/Cr: the system

In the present study, an Fe/Cr superlattice was chosen as the test system for the ANN approach. Fe/Cr multilayers are prototype systems where interlayer coupling can be observed: depending on the Cr thickness, the magnetization in subsequent Fe layers will order parallel, antiparallel or perpendicular to each other. Here, we focus on the magnetic properties of a MgO(110)/Cr(100 Å)/[Cr(11 Å)/Fe(40 Å)]$_{22}$/Cr(50 Å) superlattice, of which the magnetization vectors of the adjacent Fe layers are known to adopt an antiparallel orientation (Wang *et al.*, 1994). When an external field is applied along the easy axis of the sample, having an in-plane uniaxial anisotropy, the interlayer coupling will be affected: for small external fields the influence is negligible, but for larger external fields the antiferromagnetic coupling will be broken and the magnetization of the Fe layers will be forced towards the external field direction. Moreover, theoretical investigations have indicated that the rotation of the magnetization vectors in the Fe layers does not occur simultaneously but depends on the distance from the surface: first, the magnetization in the top Fe layer will rotate towards the external magnetic field (the so-called 'surface spin flop'), and only upon a further increase of the field will the magnetization vectors of the central laying Fe layers follow ('bulk spin flop') (Keffer & Chow, 1973; Bottyan *et al.*, 2002). The first experimental evidence of the surface spin flop transition in Fe/Cr superlattices was provided by means of magneto-optic Kerr measurements (Wang *et al.*, 1994), which probe the near-surface magnetization. For the other Fe layers, however, only the global magnetic behaviour, *i.e.* the magnetic response of the entire structure, could be measured *via* macroscopic magnetization measurements. Therefore, it is particularly interesting to investigate the influence of the external field on the orientation of the magnetization in the Fe layers as a function of depth, *i.e.* layer by layer.

A technique that is particularly suitable for this purpose is NRS of synchrotron radiation. From early Mössbauer experiments it is known that the orientation of the internal hyperfine field is strongly correlated with that of the magnetization vector **M** (Perlow *et al.*, 1960). For example, for iron, the ^{57}Fe hyperfine field is oriented antiparallel to the magnetization vector (Hanna *et al.*, 1960), and has a value of −33.0 T at room temperature (Bergmann *et al.*, 1994). The hyperfine field information that is extracted from the NRS spectra is thus directly related to the magnetization of the Fe layers. Moreover, the isotopic selectivity of the NRS technique is particularly valuable for obtaining depth-selective information: by replacing certain regions of the sample with the nuclear resonant ^{57}Fe isotope, and the other regions with the non-resonant ^{56}Fe, the magnetic properties of these sites can be measured selectively (L'abbé *et al.*, 2004).

The experimental data set analyzed in this work was collected on a [Cr(11 Å)/Fe(40 Å)]$_{22}$ multilayer, of which the third Fe layer from the surface consists of ^{57}Fe. The sample was grown by DC magnetron sputtering onto a MgO(110) substrate, as described by Fullerton *et al.* (1993). A 100 Å Cr buffer was first deposited at 673 K to improve the epitaxial growth. Subsequently, the [Cr(11 Å)/Fe(40 Å)]$_{22}$ multilayer was grown at 383 K. Finally, the whole structure was capped with 50 Å Cr to prevent oxidation. The NRS experiments were performed at beamline ID-22N of the ESRF in Grenoble, France (Rüffer & Chumakov, 1996). A 14.4 keV photon beam with a spectral width of 6 meV was reflected by the sample at a grazing angle of 3.6 mrad. An external magnetic field was applied along the σ-vector of the incoming radiation, parallel to the in-plane easy axis of the sample. To obtain a complete image of the magnetization reversal in the ^{57}Fe layer as a function of external field, an extensive set of NRS spectra were recorded for 50 different external field values, in a field range between −0.5 T and 0.5 T.

4. Fe/Cr: conventional data analysis

First, the experimental data were analyzed in the conventional way, by comparing the measured data with theoretically calculated spectra with the help of the least-square fit routine *CONUSS* (Sturhahn, 2000). In Fig. 3(*a*), a selection of the measured NRS spectra is shown. The external field significantly influences the shape of the NRS spectra, whereas for B_{ext} = 0.5 T and B_{ext} = −0.5 T the shape of the spectra is similar to the 0° simulation of Fig. 2(*d*), the 0.18 T spectrum showing a strong resemblance to the 90° simulation. This clearly indicates that the hyperfine field, and consequently the

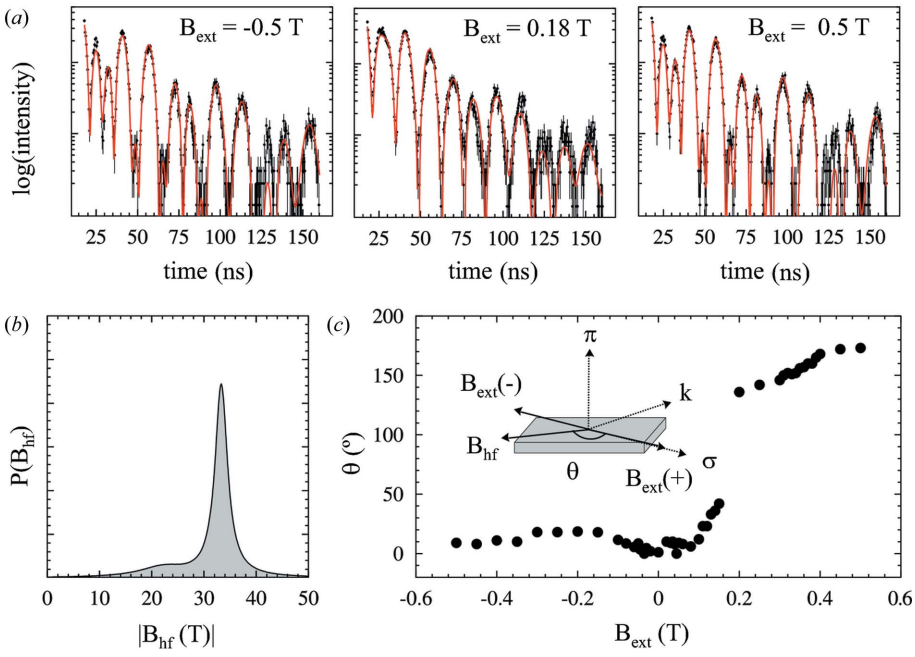

Figure 3
(*a*) Selection of the experimental data that were measured on the Fe/Cr multilayer. The solid red lines are the corresponding spectra that were calculated with the output parameters from the conventional data analysis. (*b*) Resulting hyperfine field distribution of the ^{57}Fe layer. (*c*) Experimental results for θ as a function of the applied field, determined for all spectra in the experimental data set.

magnetization in the Fe layer, rotates under the influence of the external field.

Initially, the NRS time spectra were analyzed by assuming a single magnetic hyperfine field in the ^{57}Fe layer. The rotation of the magnetic hyperfine field as a function of the external field was described by the angle θ, defined as the in-plane angle between the hyperfine field and the σ-vector of the incoming radiation. The hyperfine field was supposed to be centred around approximately -33 T, taking into account a Lorentzian distribution (with full width at half-maximum Γ). By using this model, however, significant discrepancies between the data and the calculated spectra were observed. L'abbé *et al.* (2004) and Toellner *et al.* (1995) demonstrated that additional components in the ^{57}Fe hyperfine field distribution are required in order to analyze the spectra. These components arise from the thin interface region between the ^{57}Fe layer and the adjacent Cr layers, and are characterized by a reduced hyperfine field compared with the 'core' -33 T component. In our analysis, the interface was modelled with a single hyperfine field component, of which the orientation was assumed to be the same as that of the hyperfine field in the central part (core) of the ^{57}Fe layer.

In total, six parameters were used to analyze the spectra: the angle θ, the magnitude of the core hyperfine field ($B_{\rm hf1}$), the magnitude of the interface hyperfine field ($B_{\rm hf2}$), the FWHM of both magnetic fields (Γ_1 and Γ_2, respectively), and the weight of the interface site with respect to the core site (weight$_2$). Whereas the first parameter describes the orientation of the core and the interface hyperfine fields with respect to the external field, the other five parameters determine the hyperfine field distribution of the ^{57}Fe layer. The resulting distribution is shown in Fig. 3(*b*). For the core, a magnetic hyperfine field $B_{\rm hf1}$ of -33.3 (2) T with a distribution Γ_1 of 2.9 (3) T could be extracted from the data. The interface shows a reduced hyperfine field $B_{\rm hf2}$ of -22.2 (8) T with a broad full width at half-maximum Γ_2 of 11 (2) T. The weight of the interface site was found to be 0.20 (2) times the weight of the core contribution. These values are the average values of the hyperfine field parameters that were extracted from the individual spectra separately, with the standard deviations as corresponding errors. The relatively large error on $B_{\rm hf2}$ and Γ_2 indicates a reduced sensitivity of the NRS spectra to the interface parameters: a slight change of these parameters only weakly affects the shape of the NRS spectrum.

The evolution of θ as a function of external field is illustrated in Fig. 3(*c*). It is important to note that the time spectra are sensitive to the magnitude and the direction of the hyperfine field, but not to its sign; the projection of the hyperfine field on σ can either be positive or negative (L'abbé *et al.*, 2004). For the -0.5 T measurement, for instance, θ was assumed to be 9 (2)°, but, in principle, exactly the same fit would be obtained with an angle of 171 (2)°. However, the 171 (2)° solution can be excluded for physical reasons: for a large external field of -0.5 T, the magnetization in the ^{57}Fe layer can be expected to be aligned with the applied field, so that the magnetic hyperfine field will point along the σ-vector of the incoming radiation [θ = 9 (2)°]. Around 0.15 T, the hyperfine field starts to rotate towards the direction of the incoming photon beam [θ = 37 (3)°]. This is clearly reflected in the shape of the 0.18 T measurement. Finally, for the +0.5 T measurement, the magnetization will again be fully aligned with the external field, so that the hyperfine field can be expected to be antiparallel to σ [θ = 173(2)°].

5. Fe/Cr: ANN data analysis

To investigate the capabilities of ANNs for the analysis of the experimental data, an artificial neural network was trained to determine the magnetic properties in the ^{57}Fe layer of the Fe/Cr superlattice. For our specific case, the network was constructed on the basis of the six-parameter model that was described in the previous section, with the NRS spectra as input data, and θ, $B_{\rm hf1}$, $B_{\rm hf2}$, Γ_1, Γ_2 and weight$_2$ as the desired output parameters.

For the network, a (I, 150, 75, 25, O) architecture was chosen, where I is the input layer of the ANN (250 input nodes, which are the counts per channel, for each NRS spec-

trum), *O* is the output layer of the network (six parameters), and the numbers in between are the numbers of nodes of the three hidden layers. Several other architectures were chosen by trial and error, but did not lead to a drastic improvement or deterioration of the network error. The training of the network was realised *via* the supervised learning method. To create a training set, 20000 theoretically calculated NRS spectra with randomly chosen values of the six parameters within the experimental possibilities were generated using *CONUSS*. In order to make the training set as realistic as possible, all spectra were convoluted with Poisson noise, as one would expect for experimentally obtained data. As such, numerous NRS spectra and their corresponding parameters determining the shape of the spectrum were available for the training. The generation of the training set was completed in about 5 h using a Pentium-4 computer running at 2.66 GHz, whereas the training of the network, as described in the *Introduction*, was realised in less than half an hour.

To test the performance of the trained network, an evaluation set of 200 independent NRS spectra, calculated in the same way and with the same parameter ranges as the spectra of the training set, was generated. After the neural network was applied to the evaluation set, the calculated output parameters of the ANN were compared with the target parameters (*i.e.* the original parameters by which the simulations were made) for each spectrum of the evaluation set. The results are shown in Fig. 4. The relationship between the target and output parameters of the network approaches very well the desired behaviour of an ideal ANN, *i.e.* a linear dependence with slope 1. The fact that the interface parameters seem to be slightly harder to reproduce than the core parameters again reflects the reduced sensitivity of the NRS spectra to the interface region. It should also be noted that only limited parameter ranges were used to generate the spectra of the evaluation set; for the core parameters, for instance, B_{hf1} was restricted to the region between −38 T and −30 T, whereas Γ_1 was confined between 2.2 T and 4.2 T. These are the same ranges that were used to generate the spectra of the training set, and are the maximal ranges for which a trained network could be obtained. For broader intervals, no satisfactory minimum error on the network could be reached. This indicates the limits of the artificial neural networks: when several parameters are present, each of which can significantly modify the shape of the NRS spectrum, the ANN will be inefficient to analyze the data.

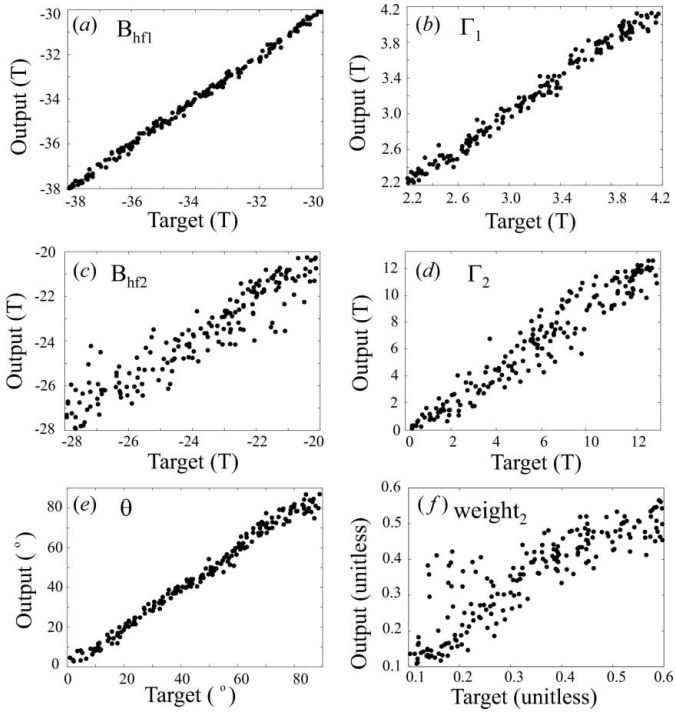

Figure 4
Comparison between the nominal parameters (target) and the output parameters of the ANN (output) for the 200 spectra of the evaluation set.

Table 1
Comparison between the output parameters from the conventional data analysis (CONV) and from the ANN analysis (ANN) for the five parameters of the ^{57}Fe hyperfine field distribution.

	B_{hf1} (T)	Γ_1 (T)	B_{hf2} (T)	Γ_2 (T)	weight$_2$ (a.u.)
CONV	−33.3 (2)	2.9 (3)	−22.2 (8)	11 (2)	0.20 (2)
ANN	−33.3 (2)	2.8 (3)	−22.2 (6)	10 (2)	0.20 (3)

After training and testing of the network, the experimental Fe/Cr data were analyzed with the ANN. The total analysis time for the 50 spectra was less than 1 s. The processing of the same data set by means of the conventional method took about 3 h. In Fig. 5(*a*), three theoretical spectra, generated from the output parameters of the ANN, are superimposed onto the experimental data. Although the agreement between calculations and experiment is slightly worse than in the case of the manual fitting [see for instance the 25 ns beat in the central panel of Fig. 5(*a*)], it is clear that the developed network allows one to reproduce the experimental data with a very high degree of fidelity. This is also illustrated in Figs. 5(*b*) and 5(*c*), where the output of the ANN is compared with the results that were obtained by the conventional data analysis. For each external field value, the ANN analysis yields a θ value that corresponds very well with the results of the conventional analysis (Fig. 5*b*). In Table 1, the average values of the five remaining parameters and their corresponding standard deviations, obtained by the two analysis methods, are compared. The overall hyperfine field distributions obtained by both methods overlap almost completely (Fig. 5*c*).

6. Conclusions

We have developed an artificial neural network for the analysis of NRS spectra that were measured on a Fe/Cr multilayer system. The network was trained by means of a theoretically generated training set, and applied to experimental NRS data with excellent results. From the six output parameters of the network, the measured spectra can be reproduced with very high accuracy. The results, which are obtained without any knowledge of the underlying physics, are in very good agreement with those of the conventional data analysis. This means that the results given by the ANN can be

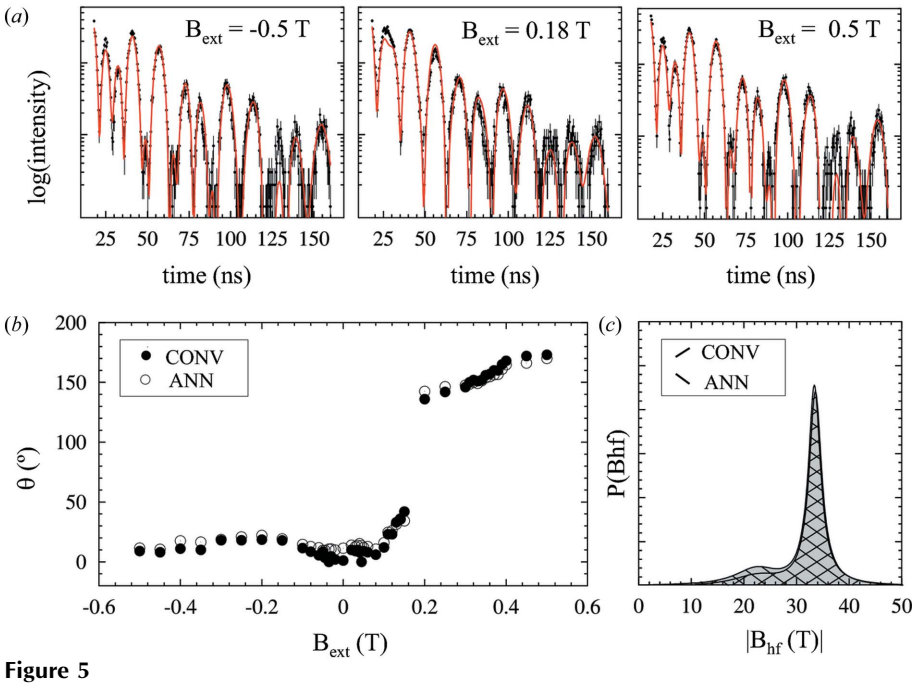

Figure 5
(*a*) Selection of the experimental data that were measured on the Fe/Cr multilayer. The solid red lines are the corresponding spectra that were calculated with the output parameters of the ANN. (*b*) Experimental results for θ, determined both from the conventional data analysis (CONV) and from the ANN analysis. (*c*) Hyperfine field distribution in the ^{57}Fe layer, obtained from the two analysis methods.

taken directly as such, or can be used as an initial guess for further refinement in *CONUSS*. While we focused in this work on the magnetic properties of one specific sample, the same network can be applied to all experimental data sets of which the relevant physical parameters lie within the experimental range of the training set. However, when broader parameter ranges are required, or when additional parameters influence the shape of the NRS spectra, a new ANN must be built and trained. This is clearly a general shortcoming of the ANN approach. On the other hand, in many NRS experiments several similar samples are measured in the same experimental run, creating a large amount of comparable spectra that can be analyzed with the same ANN. This is also the case for the Fe/Cr example: whereas the current work was limited to the magnetic properties of one selective layer of the Fe/Cr multilayer, it is certainly appealing to extend the measurements to other Fe/Cr samples, having a different Fe layer enriched with the ^{57}Fe isotope. By developing a network that takes into account both the magnetic characteristics and the structural composition of the various samples, all data sets can be analyzed with the same network.

In conclusion, the capability of artificial neural networks for a fast and accurate data analysis in NRS experiments has been demonstrated for an Fe/Cr case. We have shown that the relevant hyperfine interaction parameters can be determined fully automatically and almost instantaneously for each spectrum in the experimental data set. Given the successful results, the network can be extended to many other NRS experiments where a qualitative analysis of the data is required. Once the relevant parameters are identified and the parameter ranges are correctly set, for example by analyzing one spectrum with the conventional method, a suitable ANN can be built and trained, and subsequently applied to an extensive amount of data. Although the preparation of the analysis, *i.e.* the construction of a suitable ANN, may still be time-consuming, the effort clearly pays off when large data sets are considered. Hence, the ANN analysis method is a step forward towards an automated evaluation of NRS experiments, and could serve as inspiration to other synchrotron-based experimental methods that have to deal with an increasing amount of experimental data.

We especially wish to cordially thank R. Rüffer and the staff at the ESRF beamline ID-22N for their help during the experiment, A. Vieira for the introduction to ANNs, and S. J. Jiang and S. D. Bader for their help with facilitating the sample preparation. The work was supported by the European Community *via* STREP No. NMP4-CT-2003-001516 (DYNASYNC), by the FWO (Fund for Scientific Research Flanders), by the Concerted Action of the KU Leuven (GOA/09/006), by CREA 07/005, and by the Centers of Excellence Programme (INPAC EF/05/005).

References

Barradas, N. P. & Vieira, A. (2000). *Phys. Rev. E*, **62**, 5818–5829.
Barradas, N. P., Vieira, A. & Patrício, R. (2002). *Phys. Rev. E*, **65**, 066703.
Bergmann, U., Shastri, S. D., Siddons, D. P., Batterman, B. W. & Hastings, J. B. (1994). *Phys. Rev. B*, **50**, 5957–5961.
Bishop, C. M. (1995). *Neural Networks for Pattern Recognition.* Oxford University Press.
Bottyán, L., Deák, L., Dekoster, J., Kunnen, E., Langouche, G., Meersschaut, J., Major, M., Nagy, D. L., Ruter, H. D., Szilágyi, E. & Temst, K. (2002). *J. Magn. Magn. Mater.* **240**, 514–516.
Callens, R., L'abbé, C., Meersschaut, J., Serdons, I., Sturhahn, W. & Toellner, T. S. (2005). *Phys. Rev. B*, **72**, 081402(R).
De Souza, P. A., Garg, V. K., Klingelhöfer, G., Gellert, R. & Gütlich, P. (2002). *Hyperfine Interact.* **139/140**, 705–714.
Duponchel, L., Ruckebusch, C., Huvenne, J. P. & Legrand, P. (1999). *J. Near Infrared Spectrosc.* **7**, 155–166.
Fullerton, E. E., Conover, M. J., Mattson, J. E., Sowers, C. H. & Bader, S. D. (1993). *Phys Rev. B*, **48**, 15755–15763.
Gerdau, E., Rüffer, R., Winkler, H., Tolksdorf, W., Klages, C. P. & Hannon, J. P. (1985). *Phys. Rev. Lett.* **54**, 835–838.
Hanna, S. S., Heberle, J., Perlow, G. J., Preston, R. S. & Vincent, D. H. (1960). *Phys. Rev. Lett.* **4**, 513–515.
Keffer, F. & Chow, H. (1973). *Phys. Rev. Lett.* **31**, 1061–1063.
L'abbé, C., Meersschaut, J., Sturhahn, W., Jiang, J. S., Toellner, T. S., Alp, E. E. & Bader, S. D. (2004). *Phys. Rev. Lett.* **93**, 037201.
Mössbauer, R. L. (1958). *Z. Phys. A*, **151**, 124–143.
Paulsen, H., Linder, R., Wagner, F., Winkler, H., Pöppl, S. J. & Trautwein, A. X. (2000). *Hyperfine Interact.* **126**, 421–424.

Perlow, G. J., Hanna, S. S., Hamermesh, M., Littlejohn, C., Vincent, D. H., Preston, R. S. & Heberle, J. (1960). *Phys. Rev. Lett.* **4**, 74–75.
Röhlsberger, R. (2004). *Nuclear Condensed Matter Physics with Synchrotron Radiation: Basic Principles, Methodology and Applications.* Berlin: Springer.
Röhlsberger, R., Bansmann, J., Senz, V., Jonas, K. L., Bettac, A., Leupold, O., Rüffer, R., Burkel, E. & Meiwes-Broer, K. H. (2001). *Phys. Rev. Lett.* **86**, 5597–5600.
Röhlsberger, R., Thomas, H., Schlage, K., Burkel, E., Leupold, O. & Rüffer, R. (2002). *Phys. Rev. Lett.* **89**, 237201.
Rüffer, R. & Chumakov, A. I. (1996). *Hyperfine Interact.* **97/98**, 589–604.
Shvyd'ko, Yu. V. (1999). *Phys. Rev. B*, **59**, 9132–9143.
Sturhahn, W. (2000). *Hyperfine Interact.* **125**, 149–172.
Sturhahn, W. (2001). *Phys. Rev. B*, **63**, 094105.
Toellner, T. S., Sturhahn, W., Röhlsberger, R., Alp, E. E., Sowers, C. H. & Fullerton, E. E. (1995). *Phys. Rev. Lett.* **74**, 3475–3478.
Wang, R. W., Mills, D. L., Fullerton, E. E., Mattson, J. E. & Bader, S. D. (1994). *Phys. Rev. Lett.* **72**, 920–923.